ICAS 2016
30th Congress of the International Council
of the Aeronautical Sciences
DCC, Daejeon, Korea ; September 25-30, 2016

A COMPUTATIONAL STUDY ON AVIAN FLAPPING FLIGHT AND THE INFLUENCE OF FEATHER SEPARATION

Jeffrey Feaster, Francine Battaglia, and Javid Bayandor
CRashworthiness for Aerospace Structures and Hybrids (CRASH) Lab
Virginia Tech
Blacksburg, VA 24061 USA

Abstract

Bird flight is an area of significant interest due to the utilization and control of unsteady aerodynamic effects via flapping. Although modern aerodynamics were originally inspired by bird flight, contemporary computational and experimental work associated with flapping flight focuses on insect flight. The purpose of the present paper is to improve the understanding of avian flight by investigating upstroke downstroke velocities, feather separation, and ultimately develop a nondimensional model to predict lift and drag forces for seagull flight. The variation in upstroke-downstroke velocities were found to decrease both lift and drag as the relative upstroke velocity increased, but significantly increased the lift:drag ratio for the same flight regime. Feather separation was found to increase lift with maximum lift at a separation angle of $25°$, while drag increased linearly. A set of nondimensional equations found were using regression analysis that can be used as a design tool to predict both lift and drag without expensive experiments or excessive computational processing requirements.

1 Background and Introduction

The unsteady aerodynamic effects of bird flight is of interest to utilize and control flapping in bioinspired applications [1–3]. The ability to control flapping flight can afford opportunities to have a higher overall efficiency versus that of fixed wing flight at biological locomotive scales [4,5]. Within the realm of avian flight, there are two main wing gaits for sustained locomotion defined by the vortex structure in the wake: continuous-wake and ring-wake [6]. Most birds utilize a vortex-ring gait for acceleration, exhibiting significant vertical displacement. Depending on the size and morphology, some birds are able to utilize a continuous-vortex gait for long duration flight to improve efficiency [7,8].

There have been numerous experimental and computational studies of bird flight. Modern engineering experimental investigations of avian locomotion focused on describing and visualizing ring and continuous-wake gaits and improving the understanding of the energetics required for sustained flight [9–11]. The kinematics of morphologically different species of birds were captured at various flight velocities to gain a better understanding of the biological transition from ring-wake to continuous-wake flight, determining for some smaller birds that no transition occurred or that it only occurred in gliding scenarios [6,12–15]. The flapping transitions were found to be motivated by improvements in energetic efficiency as the flight velocity and required flight distances increased [7,8,16,17].

At present, to the authors' knowledge, avian-specific computational studies are relatively limited. Three papers investigate the effects of unsteady aerodynamics on avian flight. Willis et al. [17] compared a Betz criterion code and an unsteady, potential flow solver to determine power optimal wake structures and associated kinematics. Willis et al. [18] also investigated formation flight and ground effects on flapping aerodynamics. Han [5] utilized a panel method to describe the unsteady motion of a seagull wing to determine the effects that wing joints had on the overarching aerodynamics experienced by a seagull. Moelyadi and Sachs

[19] captured the dynamic yaw stability derivatives for a gliding seagull using the unsteady Navier-Stokes equations.

The purpose of the present paper is to improve the understanding of avian flight by investigating the effects of upstroke-downstroke velocity, feather separation, and develop a predictive set of equations for lift and drag for continuous-vortex seagull flight.

2 Kinematics

An important element to model flapping motion is the implementation of the kinematic equations. Studies have shown that kinematic modeling of a bird wing requires the simplification of the motion into two interlinked joints as shown in **Error! Reference source not found.**. The primary wing section creates thrust and lift, and the secondary section produces lift. The lift produced by the primary section is less than that of the secondary section.

The primary wing section has three degrees of freedom: flapping (roll axis), sweeping (yaw axis), and pitching. These equations are:

$$V_{2,y} = 2\pi f \psi_1 r \sin(2\pi f \Delta t)$$
$$+2\pi f \psi_2 r_2 \sin(2\pi f \Delta t) \qquad (1)$$
$$V_{2,x} = 2\pi f \phi r_2 \sin(2\pi f \Delta t) \qquad (2)$$
$$\dot{\theta}_2 = 2\pi f \theta_2 \cos(2\pi f \Delta t) \qquad (3)$$

where ψ_1 is the amplitude of the angular displacement (as shown in Fig. 1), r is the distance between the shoulder joint and the cross-section being modeled (the midpoint in all simulations), f is the flapping frequency, and Δt is the time step. The vertical velocity, $V_{2,y}$, models the flapping motion. The horizontal velocity, $V_{2,x}$, models the sweeping motion. The angular velocity, $\dot{\theta}_2$, models the pitching motion. With equations (1), (2), and (3) the kinematics of a bird wing are properly modeled using the parameters determined by Liu et al. [20].
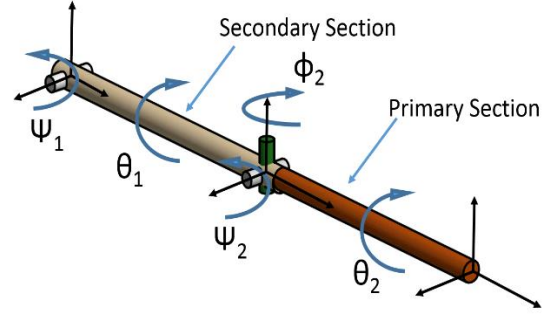
Fig. 1. Schematic for the motion of the primary and secondary wing sections.

The secondary section is modeled as a single degree of freedom at the shoulder joint, it is actually a rotational velocity since it is a[6] rotation at the shoulder, but for a two-dimensional simulation is modeled as a translational velocity. The equation for the secondary wing section motion is:

$$V_{1,y} = 2\pi f \psi_1 r_1 \sin(2\pi f t) \qquad (4)$$

where $V_{1,y}$ is the vertical translational velocity.

2 Numerical Methods

The commercial software ANSYS Fluent (v. 15) is used to solve the velocity and pressure fields around a dynamic two-dimensional wing cross-section. The unsteady, incompressible formulation of the Navier-Stokes equations is employed, yielding the continuity equation:

$$\nabla \cdot \vec{v} = 0 \qquad (5)$$

where t is time, $\vec{v}$ is the velocity vector and ρ is the fluid density. Neglecting gravitational effects, the momentum equations are:

$$\rho[\partial \vec{v}/\partial t + \vec{v} \cdot \nabla \vec{v}] = -\nabla P + \nabla \cdot \bar{\bar{\tau}} \qquad (6)$$

where P is the pressure and $\bar{\bar{\tau}}$ is the fluid stress tensor.

The segregated pressure-based Navier-Stokes (PBNS) solver is used to simulate the incompressible flow [21] using the SIMPLE algorithm for the pressure-velocity coupling. The gradients are discretized using the least squares cell based (LSCB). The momentum equations are

discretized using the second-order upwind scheme and time is discretized using a first-order implicit method. The absolute convergence criteria are set to 10^{-5}. The time step is determined using a modified version of the Courant-Fredrichs-Levy (CFL) number to suit the implementation of kinematic motion:

$$CFL = \frac{\sqrt{\{V_x^2 + V_y^2\}\Delta t}}{\Delta X} \qquad (7)$$

where ΔX is the smallest cell size.

To perform a computational analysis a mesh is generated using ANSYS ICEM. An S1223 airfoil accurately represents the cross section of both the primary and secondary bird wing sections so it is used in the CFD model [20]. In order to generate the mesh, point data is input to ICEM and the geometry is completed by connecting the points. A fluid flow region is then created around the airfoil and a triangular mesh is generated within the fluid flow region. The triangular mesh allows for dynamic meshing, which is needed to model the flapping wing.

An unstructured finite-volume mesh is generated around the cross-section and is updated with each time step to allow for proper mesh motion, using a combination of Laplacian smoothing and remeshing functions to retain mesh density around the wing at all points in time during the flapping motion. Fig. 2 shows the unstructured 2D mesh surrounding the wing profile. The fluid used in the simulations is air with a density of 1.225 kg/m^3 and dynamic viscosity of 1.79×10^{-5} kg/m-s. Air enters the computational domain along the right boundary with a uniform velocity specified. The upper and lower boundaries of the fluid domain use a slip condition. The left side of the fluid domain is specified as ambient (0 gauge pressure). The surface of the airfoil is modeled as a no-slip condition. The full domain size is $8c \times 11.6c$, where c is the airfoil chord length equal to 1.72 cm.

In order to facilitate wing motion, a dynamic mesh is used with smoothing and re-meshing so the mesh does not tear and accurate results are obtained. A diffusion smoothing factor is used for the dynamic meshing to diffuse

cell displacement along interior nodes. Re-meshing checks average cell size and displacement and adds or moves cells to maintain a consistent mesh.

2.2 Solution Validation

Grid resolution studies are performed in order to determine if the solutions are dependent on the number of cells used in a mesh. The grid convergence index (GCI) methodology is used to approximate the numerical accuracy of the solution [22]. Three meshes of increasing node density are tested: 11,309, 44,644, and 177,392 nodes. Table 1 presents the results of the GCI study, where the subscripts 3, 2 and 1 denote the coarse, medium and fine meshes. The number of nodes used guarantee a grid refine factor r greater than the required 1.3 [22]. Based on the GCI analysis, the local order of accuracy p is at least 4 and the fine-grid GCI is less than 1%. The variable tested is C_L and is denoted as Φ.

Table 1: Discretization error calculations for the airfoil.

Parameters	C_L
r21	2
r32	2
Φ_1	10.1307
Φ_2	24.9856
Φ_3	25.5828
p	4.635
GCI_{ext}^{21}	0.066%

3 Results and Discussion

3.1 Variable Flap Frequency

A literature review indicated that a variation in the velocity of the upstroke and downstroke of a wing flap could be beneficial for flight performance. The research herein involves developing a prototype and using CFD to help in the design. Thus, based on the literature, there are very few computational analyses imposing variable motion, and how it compares to a uniform flapping velocity [5,17,18,23,24]. A primary concern in this research is to conduct a

computational analysis on the effect of varying flapping velocities, specifically on the impact of lift and drag. The motivation is to determine if a variable flap velocity should be added to the prototype. Furthermore, there is a concern that a variable flap velocity could also be unintentionally produced should the prototype motor be unable to produce the correct rotation during the flap cycle. Initial efforts begin with an investigation to determine the effect of varying the ratio of the upstroke:downstroke velocity of the primary section of the wing.

Since the equations are oscillatory, a change in velocity is effectively a change in frequency. The flapping frequency for this study is 2 Hz. When implementing the variable flap velocity, it is assumed that a fast flapping frequency is greater than 2 Hz and a slow flapping frequency obeys the relationship:

$$f_s = \gamma * \frac{1}{\frac{1}{f_n} - \frac{1}{2 * f_f}} \qquad (8)$$

where f_s is the slow flapping frequency, γ is the total period of a flap, f_f is the fast flapping frequency, and f_n is the normal flapping frequency of 2 Hz. Using f_s and f_f, the motion using a UDF is implemented. The UDF identifies whether the time-step during the simulation is an upwards flap or a downwards flap, and uses the appropriate frequency, f_s or f_f.

Simulations are performed for multiple upstroke:downstroke velocity ratios that range below and above unity, specifically, ratios from 1/3 to 3. This was done to compare the impact of having a faster upstroke versus a faster downstroke. Additionally, there is interest to learn whether a trend emerges with increasing stroke ratios.

Fig. 3 and 4 present the lift and drag coefficients, respectively, for the range of velocity ratios. Similar trends are observed for both coefficients. As the velocity ratio increases, the lift and drag coefficients decrease.
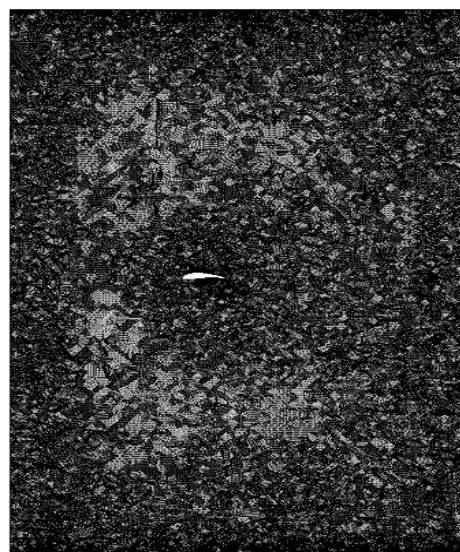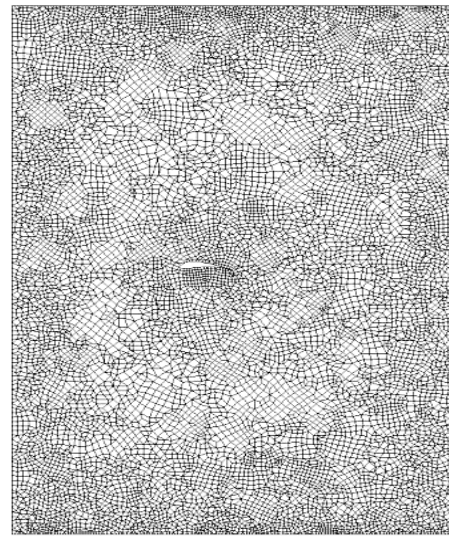
Fig. 2. Meshes for the 11,309, 44,644 and 177,392 cell cases.

Additionally, when the velocity ratio is between 1/3 and 1, both the lift and drag coefficients approach an asymptotic value that is above the value for a velocity ratio of 1. When the velocity ratios are between 1 and 3, the lift and drag coefficients seem to approach an asymptote that is below the value at a velocity ratio of 1.
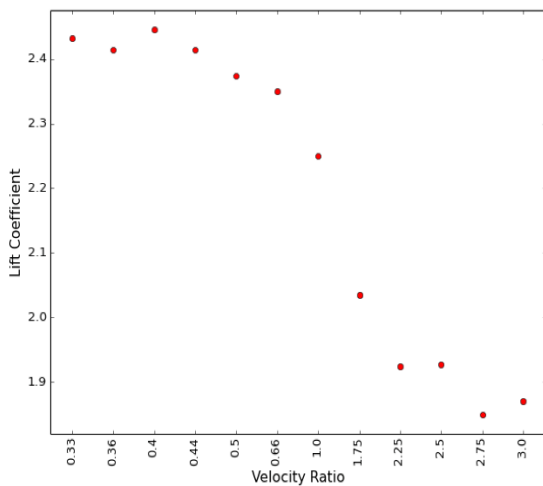
Fig. 3. Lift coefficient versus velocity ratio.

The curve for lift-to-drag ratio L/D versus velocity ratio provides another interesting observation, as seen in Fig. 5. At velocity ratios below 1, L/D remains relatively constant at a value of 17. However, at velocity ratios above 1, L/D increases dramatically with increasing velocity ratio.

Fig. 4. Drag coefficient versus velocity ratio.

The results of this study indicate that having a variable velocity ratio can be beneficial, but must be chosen with appropriate flight operating conditions corresponding to a bird. For situations in which high lift is desirable, a reduction in velocity ratio would prove beneficial. However, it is important to note that as the velocity ratio decreases, an increase in drag is also present. Thus, the impact of an increase in drag must be taken into consideration. On the other hand, drag can be dramatically reduced at velocity ratios above one, with an accompanying decrease in lift.

It is important to note that these studies do not predict how a variable flap frequency would impact thrust generation. A repetition of these studies must be performed for flight configurations that yield net thrust.

Fig. 5. L/D versus velocity ratio
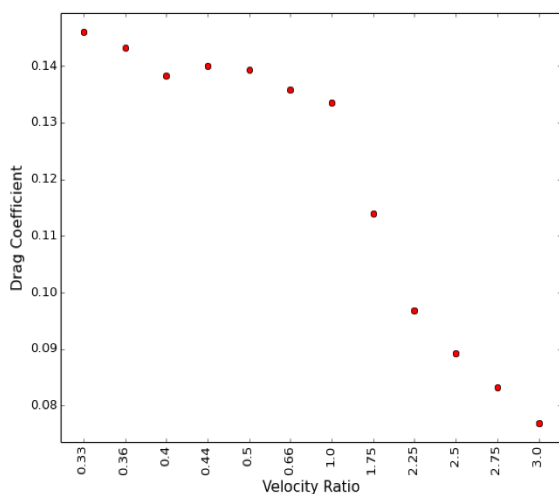
3.2 Feather Separation

An interesting feature of bird flight, for which only some species of birds can achieve, is that the wingtip feathers separate on the upstroke of the flap cycle. It is hypothesized that birds do this to allow air to flow through their feathers with less resistance on the upstroke, reducing the negative lift that is usually produced by the upstroke. The reduction of negative lift results in a more efficient flap cycle. This is only hypothesized because it is impossible to actually measure the effect of feather separation on a live bird specimen. Thus, the next part of this study will use the CFD techniques described herein to investigate feather separation in a wing.

Equations of motion were developed to allow the three feathers to remain together throughout the downstroke, separate at the beginning of the upstroke, and then close at the beginning of the downstroke. The model for feather separation is shown in Fig. 6. The image of the bird wing with feathers shows a dashed line, which represents the chord position that will be modeled. The two-dimensional model is shown in Fig. 6 to replication the wing-tip feather separation. Both macro- and micro- motion is modeled, where the macro-equations are:

$$Y = r_1 + r_2 \sin(\psi_2) \tag{9}$$
$$X = r_2 \sin(\phi_2) \tag{10}$$
$$\theta = \theta \tag{11}$$

and the micro-equations are,

$$y = c_f \sin(\theta_2) \tag{12}$$
$$x = c_f \cos(\theta_2) \tag{13}$$
$$\beta = A \sin(\omega t) \times (sgn) \tag{14}$$

where c_f represents the chord length of the feather air foil. β is used to model the rotation of the bird feather, the angle at which the feathers separate. The rotation of the bird feathers is unknown so multiple cases are simulated at different rotation angles.
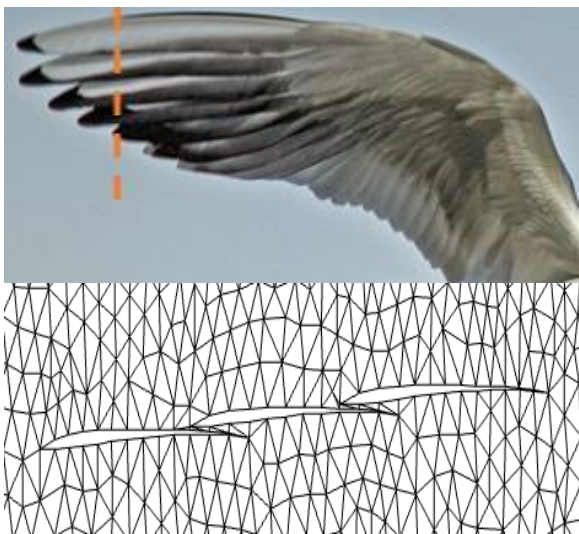
Fig. 6. (bottom) The mesh used for the separating feather study displaying the geometry resembling the actual cross-section of a bird's wingtip (top).

Four cases are simulated: three cases at separating angles of 25°, 35° and 45° and one non-separating feather case where the three feathers stay together throughout the flap cycle. The non-separating case is the base case to determine the effect of the feather separation. The separating feather cases are similar but with slightly different values. The coefficient of lift versus time and coefficient of drag versus time for the 25° separation is shown in Fig. and Fig. **,** respectively.
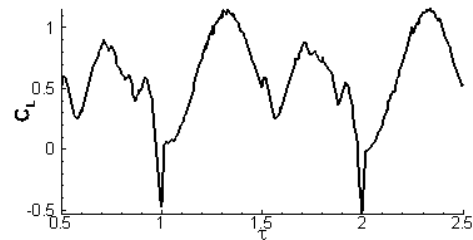
Fig. 7. The lift coefficient versus time for three flap cycles for a separating angle of 25 degrees.
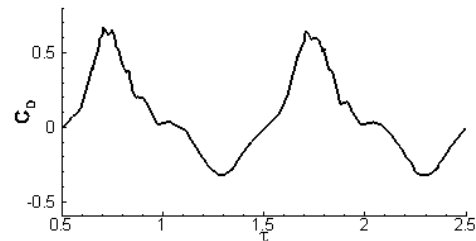
Fig. 8. The drag coefficient versus time for three flap cycles for a separating angle of 25 degrees.

From Table it is observed that the optimal separating feather case occurred at a separation angle of 25°, which produced maximum lift and minimal drag. The separating feathers increased the average coefficient of lift by a factor of 4. The separating feathers also increased the drag but since it is such a small amount of drag and only occurs at the wingtip it would not greatly affect the overall drag on the wing. From this study it is concluded that separating feathers produce lift at the wingtip and increase the overall performance of flight.

Table 2. The average lift coefficient and drag coefficient for all four cases of the feather separation study.

Degree Separation	Coefficient of Lift	Coefficient of Drag
0	0.143	-0.0164
25	0.589	0.0759
35	0.558	0.101
45	0.475	0.140

3.3 Nondimensionalization

The CFD simulations are also used to perform a parametric study to develop predictive equations for lift and drag based on nondimensionalization of key parameters of the flapping flight. The design variables are identified: air velocity (V), density (ρ), and viscosity (μ), chord length (c), amplitude in the X and Y directions (A_x & A_y), the wingtip rotation (θ), and the flapping frequency (f). It should be noted that the fluid properties (ρ, μ), chord length and velocity are not varied. Buckingham pi theorem is used to develop the nondimensional parameters. To simplify the study, A_x, is used only to derive the drag relationship, and A_y is for lift. θ is defined in radians, which already has no dimensions. To dimensionalize this variable so that it can be used to develop pi terms, the projected area from the airfoil ($C' = C\sin\theta$) gives the variable a length measurement. The pi terms will be defined using a consistent set of parameters to represent the mass, length and time scales, namely, ρ, C' and f, respectively. Table 3 summaries the pi terms for lift and drag.

Table 3. Nondimensional parameters for *L* and *D*

Variable	Π Term	Value
L D	Π_1	$L/C'^4 f^2 \rho$ $D/C'^4 f^2 \rho$
V	Π_2	$V/C'f$
C	Π_3	C/C'
μ	Π_4	$\mu/C'^2 f \rho$
A_y A_x	Π_5	A_y/C' A_x/C'

It was determined that Π_3 is not important because it only gave the angle θ that has been used as a variable to create C'. Π_5 was

also deemed unimportant due to the fact that the simplicity as a nondimensional length scale was unaffected because chord length remained constant.

Linear regression is used to construct a mathematical equation that will predict the lift or drag with known parameters of a given situation. The predictive equation for lift is:

$$\Pi_1 = \chi \Pi_2{}^\alpha \Pi_3{}^\beta + \xi \Pi_2{}^\gamma \Pi_3{}^\delta + \zeta \qquad (15)$$

For the drag relationship, the best fit equation consisted of an extra term:

$$\Pi_1 = \chi \Pi_2{}^\alpha \Pi_3{}^\beta + \xi \Pi_2{}^\gamma \Pi_3{}^\delta + \varpi \Pi_2{}^\varepsilon \Pi_3{}^\sigma + \zeta \qquad (16)$$

The coefficients and exponents (Greek variables) are solved using Mathematica, and the final equations for lift and drag, respectively, are:

$$\Pi_D = -0.41 \Pi_2{}^{2.93} \Pi_4{}^{0.24} + 1.94 \Pi_2{}^{3.01} \Pi_4{}^{0.44} + 1.02 \Pi_2{}^{1.27} \Pi_4{}^{1.05} - 0.03 \qquad (17)$$

$$\Pi_L = 14.13 \Pi_2{}^{-1.57} \Pi_4{}^{-0.89} + 15.3 \Pi_2{}^{2.69} \Pi_4{}^{0.66} + 2.84 \qquad (18)$$

To demonstrate the accuracy of the predictive relationships, the lift and drag data from the CFD simulations are compared to the results using Eq. 17 and Eq. 18, shown in Fig. 9 and Fig. 10, respectively. The linear line is the ideal relationship and the data is very tight along the line, which indicates that the equations can be used to predict the performance of the bird.
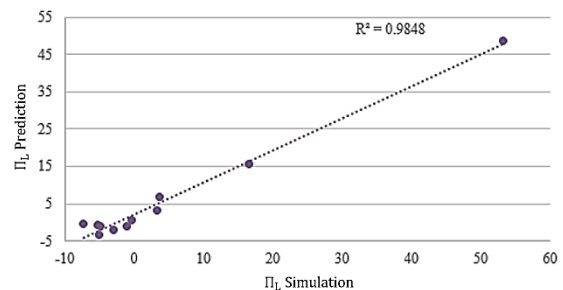
Fig. 9. The graphical representation of the simulation PI term and the predicted PI term for lift. The almost linear relationship shows that the equation is accurate.
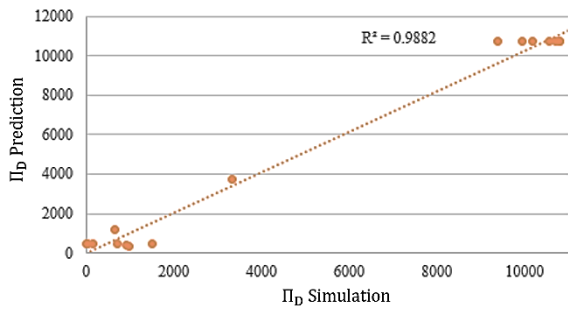
Fig. 10. The graphical representation of the simulation PI term and the predicted PI term for lift. The almost linear relationship shows that the equation is accurate.

4 Conclusion

The purpose of the present paper was to improve the understanding of avian flight by investigating the effects of upstroke-downstroke velocities, feather separation, and to ultimately develop a predictive set of equations for C_L and C_D for continuous-vortex seagull flight.

 The variations in bird flight kinematics, such as the velocities for the upstroke and downstroke, were found to have a significant effect on lift and drag. C_L and C_D were both found to decrease as the velocity of the upstroke increased relative to the downstroke velocity. Conversely, L/D remained roughly constant while the velocity of the downstroke was higher, but increased significantly once the upstroke velocity was larger.

 The separation of feathers was modeled for relative angles of $0°, 25°, 35°,$ and $45°$. The feather separation resulted in a maximum for C_L at a separation around $25°$, while C_D increased linearly.

 Nondimensional equations were derived for lift and drag using parameters of the working fluid, wing geometry and kinematics. The predictive equations agreed well with the simulation results. The important contributions of this work are the first CFD study to examine feather separation and the development of predictive equations for lift and drag that can be used in design analyses for flapping flight associated with seagulls.

References

[1] Gomez, J. C., Bryant, M. J., and Garcia, E., 2013, "Unsteady aerodynamics in ornithopter flight," **8686**, p. 868610.

[2] Hubel, T., and Tropea, C., 2006, "Experimental Investigation of a Flapping Wing Model : Some Challenges From Unsteady Aerodynamics," Aerospace, pp. 1–10.

[3] Ghommem, M., 2011, "Modeling and Analysis for Optimization of Unsteady Aeroelastic Systems," pp. 1–192.

[4] Paranjape, A. A., Dorothy, M. R., Chung, S. J., and Lee, K. D., 2012, "A flight mechanics-centric review of bird-scale flapping flight," International Journal of Aeronautical and Space Sciences, **13**(3), pp. 267–282.

[5] Han, C., 2009, "Investigation of Unsteady Aerodynamic Characteristics of a Seagull Wing in Level Flight," Journal of Bionic Engineering, **6**(4), pp. 408–414.

[6] Tobalske, B., and Dial, K., 1996, "Flight kinematics of black-billed magpies and pigeons over a wide range of speeds," The Journal of experimental biology, **199**(Pt 2), pp. 263–80.

[7] Tobalske, B. W., 2007, "Biomechanics of bird flight.," The Journal of experimental biology, **210**(Pt 18), pp. 3135–3146.

[8] Shamoun-Baranes, J., and van Loon, E., 2006, "Energetic influence on gull flight strategy selection.," The Journal of experimental biology, **209**(Pt 18), pp. 3489–3498.

[9] Rayner, J. M. V, 1978, "A new approach to animal flight mechanics," Journal of Experimental Biology, **80**, pp. 17–54.

[10] Rayner, J. M. V., 1985, "Bounding and

undulating flight in birds," Journal of Theoretical Biology, **117**(1), pp. 47–77.

[11] Spedding, G. R., 1987, "The wake of a kestrel (Falco tinnunculus) in flapping flight," The Journal of Experimental Biology, **127**, pp. 59–78.

[12] Tobalske, B., Peacock, W., and Dial, K., 1999, "Kinematics of flap-bounding flight in the zebra finch over a wide range of speeds," The Journal of experimental biology, **202 (Pt 13**, pp. 1725–39.

[13] Poore, S. O., Sánchez-Haiman, A., and Goslow, G. E., 1997, "Wing upstroke and theevolution of flapping flight," Nature, **387**(6635), pp. 799–802.

[14] Tobalske, B., and Dial, K., 1994, "Neuromuscular Control and Kinematics of Intermittent Flight in Budgerigars (Melopsittacus Undulatus)," The Journal of experimental biology, **187**, pp. 1–18.

[15] Park, K. J., Rosén, M., and Hedenström, a, 2001, "Flight kinematics of the barn swallow (Hirundo rustica) over a wide range of speeds in a wind tunnel.," The Journal of experimental biology, **204**(Pt 15), pp. 2741–2750.

[16] Tobalske, B. W., Hedrick, T. L., Dial, K. P., and Biewener, A. A., 2003, "Comparative power curves in bird flight," Nature, **421**(January), pp. 363–366.

[17] Willis, D., Peraire, J., Drela, M., and White, J., 2006, "A Numerical Exploration of Parameter Dependence in Power Optimal Flapping Flight," 24th AIAA Applied Aerodynamics Conference, (June), pp. 1–31.

[18] Willis, D., Peraire, J., and Breuer, K., 2007, "A Computational Investigation of Bio-Inspired Formation Flight and Ground Effect," 25th AIAA Applied Aerodynamics Conference, (June), pp. 1–35.

[19] Moelyadi, M. a., and Sachs, G., 2007, "CFD Based Determination of Dynamic Stability Derivatives in Yaw for a Bird," Journal of Bionic Engineering, **4**(4), pp. 201–208.

[20] Liu, T., Kuykendoll, K., Rhew, R., and Jones, S., 2006, "Avian Wing Geometry and Kinematics," AIAA Journal, **44**(5), pp. 954–963.

[21] \rmANSYS Incorporated, 2014, Fluent 15.0 User's Guide.

[22] Celik, I. B., Ghia, U., Roache, P. J., Freitas, C. J., Coleman, H., Raad, P. E., and others, 2008, "Procedure for estimation and reporting of uncertainty due to discretization in CFD applications," ASME Journal of Fluids Engineering, **130**(7), p. 078001.

[23] Gopalakrishnan, P., 2008, "Unsteady Aerodynamic and Aeroelastic Analysis of Flapping Flight," p. 208.

[24] Wang, Z. J., 2000, "Vortex shedding and frequency selection in flapping flight," Journal of Fluid Mechanics, **410**, pp. 323–341.

5 Contact Author Email Address

mailto:bayandor@vt.edu

6 Copyright Statement